J. Fluid Mech. (1983), *vol.* 131, *pp.* 401–426
Printed in Great Britain

The hybrid model and its application for studying free expansion

By G. J. PERT

Department of Applied Physics, University of Hull, Hull HU6 7RX, U.K.

(Received 14 September 1981 and in revised form 4 February 1983)

The existence of modes of compressible fluid flow involving a separation of variables into a similarity solution in two dimensions and one-dimensional flow in the third is demonstrated. The numerical integration of such flows by a modified von Neumann–Richtmyer scheme is proposed, and the stability conditions investigated, showing that a generalized Courant–Friedrichs–Lewy condition is necessary. The inclusion of dissipation in the forms of artificial viscosity and thermal conduction into the model is discussed. The results of some test calculations are presented to demonstrate the behaviour of this model.

1. Introduction

The numerical simulation of compressible gas flow is a problem of severe complexity, demanding both of computational time and store. In consequence use is generally made of symmetry to reduce the number of dimensions treated in the problem. In this paper an alternative approach is considered for simplifying the problem. The flow is reduced to an analytic form in one or more dimensions by the use of self-similar forms, the flow in the remaining directions being calculated by a cell method. Although only one such problem is considered here, it is likely that other such solutions exist and that the method is applicable to other problems.

To this end we first show that there exists an exact solution of the equations of fluid mechanics in which a body of gas possessing a similarity density profile in the (x, y)-plane, but varying in z, and of uniform temperature over that plane expands into vacuum, maintaining its self-similar form in (x, y) and with a one-dimensional form of expansion in the z-direction. Such a flow is clearly a combination of a self-similar flow and a one-dimensional expansion, and we have therefore called it a 'hybrid' flow.

The numerical integration of the hybrid model is readily accomplished by an extension of the well-known von Neumann–Richtmyer Lagrangian scheme for one-dimensional gas flow. The finite-difference forms of the governing differential equations are established, and their stability conditions examined.

The hybrid model remains an academic exercise unless it can be applied to some useful physical problems. In particular, the expansion of non-uniformly heated cylinders of general cross-section provides such a problem. If the initial length of the cylinder (in the z-direction) is long compared with the transverse (x, y) dimensions, the flow will rapidly assume a similarity form in the (x, y)-plane. Furthermore, if the temperature is initially isothermal, or if the gas is uniformly heated, the temperature remains uniform across the (x, y)-plane. We have shown (Pert 1980) that, for one-dimensional cylindrical and spherical flows, the self-similar solution gives an accurate representation of the flow, provided that the appropriate matching parameter between the initial scale lengths of the cylinder and the self-similar flow is used. In

this work we shall assume that this hypothesis can be applied to these flows, and shall use matching parameters derived in our earlier publications.

The model is applied to some real flows of this type in §11 as a demonstration of its use and as a test of its accuracy.

δz

2. The hybrid model

We consider the expansion (or contraction) of a body of gas subject to a velocity distribution within the gas of the following form. The velocities (u, v) in the (x, y)-plane are assumed to take a linear self-similar form separable in the coordinates (x, y) and (z, t), namely

$$u = \frac{xU}{X}, \quad v = \frac{yV}{Y}, \tag{1}$$

where the scale lengths X, Y are functions of time t only, and the scale velocities

$$U = \frac{\mathrm{d}X}{\mathrm{d}t}, \quad V = \frac{\mathrm{d}Y}{\mathrm{d}t}. \tag{2}$$

The axial (z) velocity component is assumed to be uniform over the (x, y)-plane and is a function of (z, t) only. It follows from (1) and (2) that the Lagrangian coordinates $(\xi_x = x/X, \xi_y = y/Y)$ remain constant for each fluid particle.

Consider a small cell fixed in the fluid of dimensions δx, δy and δz. Since w is a function of (z, t) alone, the spacing δz is independent of (x, y). The mass of the cell is constant:

$$\rho\, \delta x\, \delta y\, \delta z = \rho(XY\, \delta z)\, \delta\xi_x\, \delta\xi_y = \text{const.} \tag{3}$$

Since $XY\, \delta z$ is a function of (z, t) alone, the density distribution is separable:

$$\rho = \rho_0(z, t) f(\xi_x, \xi_y). \tag{4}$$

Furthermore, it follows from (1) that ρ must be even in (x, y), and therefore

$$\rho = \rho_0(z, t) f(\xi_x^2, \xi_y^2). \tag{4a}$$

By consideration of Euler's equation in the (x, y)-plane it follows that the pressure must be separable:

$$p = p_0(z, t)\, \phi(\xi_x^2, \xi_y^2), \tag{5}$$

where

$$p_0(z, t) = \tfrac{1}{2}\lambda_x \rho_0(z, t)\, X \frac{\mathrm{d}U}{\mathrm{d}t} = \tfrac{1}{2}\lambda_y \rho_0(z, t)\, Y \frac{\mathrm{d}V}{\mathrm{d}t}, \tag{6}$$

$$f(\xi_x^2, \xi_y^2) = -\lambda_x \frac{\partial[\phi \xi_x^2, \xi_y^2)]}{\partial \xi_x^2} = -\lambda_y \frac{\partial[\phi(\xi_x^2, \xi_y^2)]}{\partial \xi_y^2}, \tag{7}$$

where λ_x and λ_y are separation constants.

The z-component of Euler's equation has the form

$$\frac{\partial w}{\partial t} + w \frac{\partial w}{\partial z} = -\frac{\phi(\xi_x^2, \xi_y^2)}{f(\xi_x^2, \xi_y^2)} \frac{1}{\rho_0(z, t)} \frac{\partial p_0(z, t)}{\partial z}, \tag{8}$$

which is only consistent with the hypothesis $w = w(z, t)$ if the functions $f(\xi_x^2, \xi_y^2)$ and $\phi(\xi_x^2, \xi_y^2)$ are identical to within a constant factor, i.e. if the ratio p/ρ is dependent on (z, t) only. Furthermore, since X and Y are functions of time only, it follows from (6) that p/ρ must be everywhere constant. For an ideal gas this condition is upheld if the temperature is everywhere uniform. This requirement is equivalent to the usual isothermal condition as applied to uniformly self-similar flows (Pert 1974) and

maintained either adiabatically or in the case of external heating by strong thermal conduction. In this case it follows from (7) that the self-similar distribution must take a Gaussian form

$$f(\xi_x^2, \xi_y^2) = \phi(\xi_x^2, \xi_y^2) = \exp\{-(\xi_x^2 + \xi_y^2)\} \tag{9}$$

for the case $\lambda_x = \lambda_y = 1$, where X and Y are the 1/e widths of the distribution.

In view of this result it is convenient to define the 'total' temperature T_A by the ratio of pressure to density according to the ideal gas law

$$\frac{p}{\rho} = \frac{R_g}{M} T_A, \tag{10}$$

where M is the molecular mass number and R_g the gas constant. For example in a plasma

$$T_A = T_i + ZT_e, \tag{10a}$$

where T_i and T_e are the ion and electron temperatures respectively and Z the ionic charge. Clearly the hybrid condition requires that T_A be uniform everywhere.

In a similar fashion it can be shown that a mass of gas with a separable density distribution, Gaussian in (x, y) and at rest, whose 'total' temperature is always constant over the entire fluid will expand in a hybrid fashion.

The equations of motion follow from (6) and (8):

$$X\frac{dU}{dt} = Y\frac{dU}{dt} = \frac{2R_g}{M} T_A, \tag{11}$$

$$\frac{\partial w}{\partial t} + w\frac{\partial w}{\partial z} = -\frac{1}{\rho_0(z,t)}\frac{\partial p_0(z,t)}{\partial z}. \tag{12}$$

The 'total' temperature is determined from the overall energy in the gas. Thus the average thermal energy per unit mass of a polytropic gas of adiabatic index γ is

$$E_t = C_V T_A = \frac{1}{\gamma - 1}\frac{R_g}{M} T_A, \tag{13}$$

and the average kinetic energy per unit mass is

$$E_\kappa = \tfrac{1}{4}(U^2 + V^2) + \tfrac{1}{2}w^2, \tag{14}$$

averaged over the (x, y)-plane. Thus the total energy per unit mass is

$$E = \tfrac{1}{2}\{w^2 + \tfrac{1}{2}(U^2 + V^2)\} + \frac{1}{2(\gamma-1)} X\frac{dU}{dt}. \tag{15}$$

The overall energy balance is completed by including terms associated with energy deposition by external sources.

3. The local hybrid approximation

The hybrid model provides a useful solution of problems for which its condition of validity is appropriate, namely that T_A be everywhere uniform. However, in many applications we consider the flow of a system of initially large aspect ratio. In this case we may imagine that an approximately self-similar flow will be rapidly established locally in the short dimensions of the system, the flow in the long dimension (z) being relatively slow. Provided the gradients in this long dimension are relatively small we may relax the hybrid condition to apply in the (x, y)-plane only, with weak variations in X, Y and T_A with z permitted.

Under this approximation we consider $w(z,t)$ to be the velocity of flow in the z-direction averaged over the (x,y)-plane, so that there is no net flow through an (x,y)-plane moving with velocity w. We assume that the self-similar distribution is established over the (x,y)-plane sufficiently rapidly that the changes in the distribution due to the variation of the z-component of velocity with x and y are always negligible. The assumption is therefore made that the flow in the (x,y)-plane is everywhere locally self-similar with characteristic parameters X, Y, U and V which vary from plane to plane, i.e. with z as well as t.

The equations of motion are then most easily obtained by considering the flow of the fluid contained between two parallel (x,y)-planes separated by a distance δz. Equations (4) and (6) follow directly under the assumption of local similarity by a similar argument to that given earlier. The local hybrid approximation, however, unlike the hybrid model, is not exact, for in this case the analysis of (8) shows that the z-component of velocity varies across the (x,y)-plane due to the variation of X and Y with z. The appropriate equation of motion for w is obtained from the consideration of the momentum balance of the line element δz, which after integration over the (x,y)-plane yields

$$\frac{\partial w}{\partial t}+w\frac{\partial w}{\partial z}=-\frac{1}{XY\rho_0}\frac{\partial}{\partial z}[XYp_0]. \tag{12a}$$

In this case the 'total' temperature T_A varies with both z and t, but is constant across the plane (x,y). Hence no thermal energy is convected across an (x,y)-plane moving with velocity w. The energy balance is constructed in a similar manner as for the hybrid model itself, namely the average energy/unit mass across the plane (x,y) is

$$E=\tfrac{1}{2}\{\tfrac{1}{2}(U^2+V^2)+w^2\}+\frac{1}{2(\gamma-1)}X\frac{\partial U}{\partial t}, \tag{15a}$$

and is completed by including terms associated with energy deposition by external sources, and thermal conduction. We may remark that the term in w^2 in (15a) is identified by evaluating the work done by the pressure on the line element δz, namely $\partial(XYp_0)/\partial z$ and using (12a).

As noted earlier, the error in the local hybrid approximation arises from the variations of X and Y with z, which give rise to variations in the z-component of velocity across the plane (x,y). It is readily shown in cases of practical interest that the velocity varies monotonically with ξ_x and ξ_y, and furthermore that w given by (12a) is in fact the velocity at the 1/e point. In contrast, the velocity w' calculated by (12) is that at the symmetry axis of the similarity profile. Thus $w-w'$ gives a measure of the total velocity variation across the (x,y)-plane. We may therefore assess the validity of the hybrid approximation during a calculation by requiring the variation $|(w-w')/w|$ to be less than some prescribed limit.

In most simulations of the type proposed for this model this condition is upheld. Using the numerical schemes to be described later we have calculated the error due to this local approximation during the expansion of uniform cylinders of various aspect ratios. As expected, the largest error occurs in the asymptotic, late-time motion. We find that generally the fractional error is reasonably constant over the bulk of the flow, but increases towards the end (figure 1). These results are summarized in figure 2. For expansions involving aspect ratios greater than 1 the bulk error is $\approx 10^{-3}$, and only exceeds 10^{-2} in the endmost cell, whose differencing is in any case poor. For small aspect ratios the end error is more extensive, but by no means severe, and in the bulk only of order 5×10^{-5}. For very large and very small

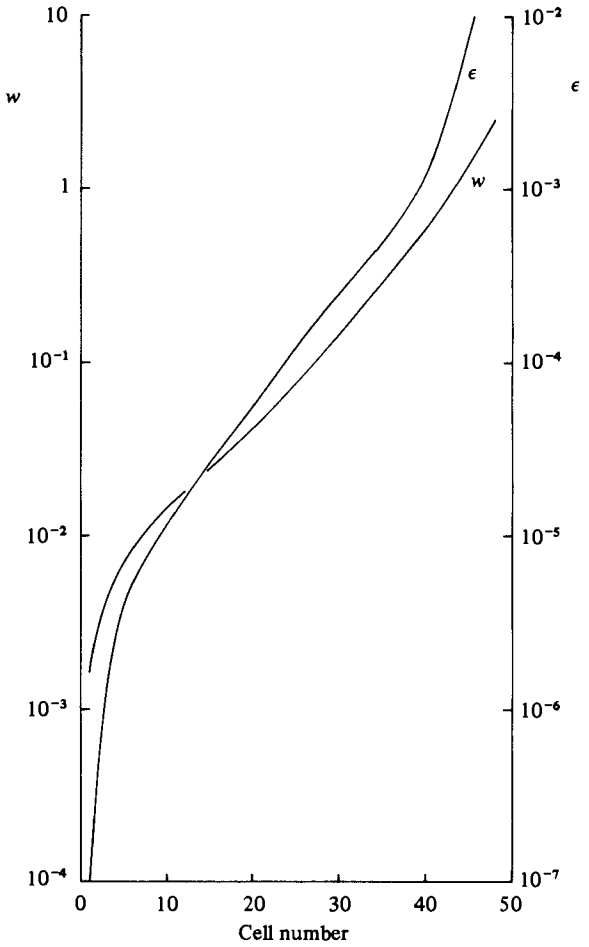

FIGURE 1. Plot of the absolute local error $\epsilon = |w-w'|$ and axial velocity w as functions of the Lagrangian cell number in the asymptotic phase of the expansion of cylinder of initial radius 1 unit and half-length 5 units. The initial energy/unit mass was 1 unit.

aspect ratios, the error is nearly independent of the ratio; indeed at a ratio of 100 the error only exceeds 1 % in the endmost cell. Results from other simulations involving heating etc. show similar behaviour, but the error is in general smaller than in the initially heated flow described here.

The nature of the simplification in the local approximation is comparable to that made in the representation of block (test) masses by a similarity model discussed in our earlier paper (Pert 1980). Indeed, since we seek to model such structures here, it is clear that the inaccuracy introduced by the local approximation is no more severe than that due to the use of a similarity expansion in (x, y) itself.

In the absence of thermal conduction along the cylinders the set of partial differential equations form a set of quasilinear hyperbolic equations. The characteristic speeds are easily shown to be $(w-c, w, w$ and $w+c)$, where c is the sound speed. The solutions to these equations can therefore be obtained by the method of characteristics. Such a procedure is, however, complex and we shall not pursue it here, preferring to develop a simple finite-difference approach.

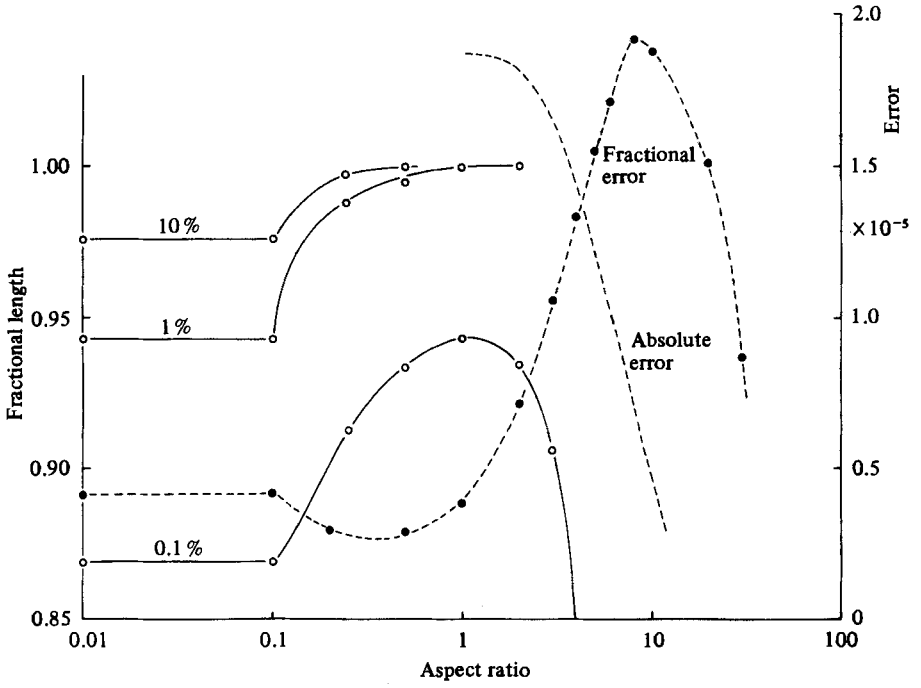

FIGURE 2. Variation of the local error with aspect ratio for conditions similar to those in figure 1. The fractional and absolute errors are measured at cell 25, and the positions of the 0.1%, 1.0% and 10.0% fractional error points estimated from the fixed centre. 48 cells were used in these calculations.

4. Shocks

The isothermal, linear self-similar form of the hybrid model has the important property of including shocks lying in the (x, y)-plane and propagating in the z-direction. The upstream state immediately ahead of the shock has a uniform temperature and Gaussian distribution of pressure and density across the shock front. Consequently the sound speed and therefore the Mach number is uniform over the (x, y)-plane in front of the shock. Since the gas is polytropic, the temperature, density and pressure ratios are uniform (Courant & Friedrichs 1948, p. 148). The downstream temperature is therefore uniform, and the pressure and density Gaussian across the (x, y)-plane.

5. Eulerian formulation

We may put these equations of motion in an Eulerian form. Thus let m be the effective fluid mass per unit length in the z-direction. Then the equation of continuity takes the form:

$$\frac{\partial m}{\partial t}+\frac{\partial}{\partial z}(mw)=0, \quad \rho_0=\frac{m}{XY}. \tag{16}$$

The kinematic equations of motion

$$\frac{\partial X}{\partial t}+w\frac{\partial X}{\partial z}=U, \quad \frac{\partial V}{\partial t}+w\frac{\partial Y}{\partial z}=V \tag{17}$$

determine X and Y. In a similar fashion the dynamic equations take the form

$$\left.\begin{aligned} \frac{\partial U}{\partial t}+w\frac{\partial U}{\partial z}=\frac{2}{X}\frac{p_0}{\rho_0}, \quad \frac{\partial V}{\partial t}+w\frac{\partial V}{\partial z}=\frac{2}{Y}\frac{p_0}{\rho_0}, \\ \frac{\partial w}{\partial t}+w\frac{\partial w}{\partial z}=-\frac{1}{m}\frac{\partial}{\partial z}(XYp_0). \end{aligned}\right\} \tag{18}$$

The equation of energy balance is

$$\frac{\partial}{\partial t}(mE)+\frac{\partial}{\partial Z}\left(m\left[E+\frac{p_0}{\rho_0}\right]\right)=m\left(W-\frac{\partial Q}{\partial z}\right), \tag{19}$$

where W is the energy deposition rate per unit mass by external sources and Q an average thermal conduction heat flux in the z-direction.

6. Lagrangian formulation

The equations of motion assume a simpler form in Lagrangian geometry. Thus consider the fluid cell defined by two neighbouring planes (x, y) of separation Δz, at the point x. Let the effective mass of the cell be $M = m\Delta z$. The equation of continuity is

$$\rho_0(z,t)=\frac{M}{XY\Delta z}, \tag{20}$$

with kinematic equations

$$\frac{\partial X}{\partial t}=U, \quad \frac{\partial Y}{\partial t}=V, \quad \frac{\partial z}{\partial t}=w, \quad \frac{\partial(\Delta z)}{\partial t}=\frac{\partial w}{\partial z}. \tag{21}$$

The dynamic equations of motion become

$$\frac{\partial U}{\partial t}=\frac{2}{X}\frac{p_0}{\rho_0}, \quad \frac{\partial V}{\partial t}=\frac{2}{Y}\frac{p_0}{\rho_0}, \quad \frac{\partial w}{\partial t}=-\frac{1}{M}\frac{\partial}{\partial z}(XYp_0). \tag{22}$$

The equation of energy balance is

$$\frac{\partial E_t}{\partial t}+p_0\frac{\partial \tau_0}{\partial t}=W-\frac{\partial Q}{\partial z}, \tag{23}$$

where E_t is the thermal energy given by (13) and τ_0 the specific volume on axis, $\tau_0 = 1/\rho_0$.

7. Finite-difference integration

The Lagrangian form of these equations is readily integrated by a simple generalization of the well-known von Neumann–Richtmyer scheme (Richtmyer & Morton 1967) for solving one-dimensional fluid problems in Lagrangian geometries. To this end the equations are integrated explicitly using a leapfrog technique where the densities and pressures are evaluated one half timestep out of phase with the velocities.

To apply this scheme to the hybrid model, we divide the gas into cells in the z-direction, a cell being the gas initially lying between the planes z_i and z_{i+1}. We define the state variables, pressure, density and temperature at the cell centre and at integer time steps, together with the similarity variables X and Y. The similarity velocities

U and V are defined at the cell centres but at half-integer timesteps. As in most schemes the cell coordinate z_i is defined at the cell boundary at integer timesteps, and the boundary velocity at the same point but at half-integer timesteps. The set of variables is thus

$$\left.\begin{gathered} p^n_{i+\frac{1}{2}},\quad \rho^n_{i+\frac{1}{2}},\quad T^n_{i+\frac{1}{2}},\quad X^n_{i+\frac{1}{2}},\quad Y^n_{i+\frac{1}{2}},\quad \tau^n_{i+\frac{1}{2}}=\frac{1}{\rho^n_{i+\frac{1}{2}}},\quad E^n_{ti+\frac{1}{2}}=C_v T^n_{i+\frac{1}{2}},\\ U^{n+\frac{1}{2}}_{i+\frac{1}{2}},\quad V^{n+\frac{1}{2}}_{i+\frac{1}{2}},\quad Z^n_i,\quad W^{n+\frac{1}{2}}_i. \end{gathered}\right\} \tag{24}$$

The finite-difference equations are identical with those for the von Neumann–Richtmyer scheme (Morton & Richtmyer 1967, p. 295) with appropriate additions:

$$U^{n+\frac{1}{2}}_{i+\frac{1}{2}} = U^{n-\frac{1}{2}}_{i+\frac{1}{2}} + \frac{2\Delta t\, p^n_{i+\frac{1}{2}}}{X^n_{i+\frac{1}{2}}\rho^n_{i+\frac{1}{2}}}, \tag{25}$$

$$V^{n+\frac{1}{2}}_{i+\frac{1}{2}} = V^{n-\frac{1}{2}}_{i+\frac{1}{2}} + \frac{2\Delta t\, p^n_{i+\frac{1}{2}}}{Y^n_{i+\frac{1}{2}}\rho^n_{i+\frac{1}{2}}}, \tag{26}$$

$$W^{n+\frac{1}{2}}_i = W^{n-\frac{1}{2}}_i - \frac{2\Delta t[X^n_{i+\frac{1}{2}}\, Y^n_{i+\frac{1}{2}} p^n_{i+\frac{1}{2}} - X^n_{i-\frac{1}{2}}\, Y^n_{i-\frac{1}{2}} p^n_{i-\frac{1}{2}}]}{M_{i-\frac{1}{2}} + M_{i+\frac{1}{2}}}, \tag{27}$$

$$X^{n+1}_{i+\frac{1}{2}} = X^n_{i+\frac{1}{2}} + U^{n+\frac{1}{2}}_{i+\frac{1}{2}}\Delta t, \tag{28}$$

$$Y^{n+1}_{i+\frac{1}{2}} = Y^n_{i+\frac{1}{2}} + V^{n+\frac{1}{2}}_{i+\frac{1}{2}}\Delta t, \tag{29}$$

$$Z^{n+1}_i = Z^n_i + W^{n+\frac{1}{2}}_i\Delta t, \tag{30}$$

$$\tau^{n+1}_{i+\frac{1}{2}} = \frac{X^{n+1}_{i+\frac{1}{2}}\, Y^{n+1}_{i+\frac{1}{2}}(Z^{n+1}_{i+1} - Z^n_i)}{M_{i+\frac{1}{2}}}, \tag{31}$$

$$E^{n+1}_{ti+\frac{1}{2}} = E^n_{ti+\frac{1}{2}} - \tfrac{1}{2}(p^{n+1}_{i+\frac{1}{2}} + p^n_{i+\frac{1}{2}})(\tau^{n+1}_{i+\frac{1}{2}} - \tau^n_{i+\frac{1}{2}}). \tag{32}$$

This scheme is clearly centred difference and therefore second order. It maintains the positivity of density and energy provided that

$$\left.\begin{gathered} (W^{n+\frac{1}{2}}_i - W^{n+\frac{1}{2}}_{i+1})\Delta t < z^n_{i+1} - z^n_i,\\ \frac{\gamma-1}{\gamma+1} < \frac{\tau^{n+1}_{i+\frac{1}{2}}}{\tau^n_{i+\frac{1}{2}}} < \frac{\gamma+1}{\gamma-1}, \end{gathered}\right\} \tag{33}$$

both of which place a constraint upon the timestep Δt. Furthermore, we demonstrate in appendix A that the scheme is weakly conservative (Pert 1981) in energy, which thereby places an upper bound on the solution provided a conservation error limit is placed on the timestep. The scheme is therefore formally stable (Pert 1981). It is not necessarily well behaved, for there may exist linearly unstable modes which are nonlinearly damped, but are nonetheless undesirable. To maintain the solution linearly stable we show in appendix B that it is necessary to introduce a Courant–Friedrichs–Lewy timestep constraint to the similarity flow in addition to that along the z-axis, namely

$$(c\Delta t)^2\left\{\frac{1}{2X^2_{i+\frac{1}{2}}} + \frac{1}{2Y^2_{i+\frac{1}{2}}} + \frac{1}{\Delta z^2_{i+\frac{1}{2}}}\right\} \leqslant 1. \tag{34}$$

These conditions on Δt themselves provide the necessary conservation error limit on Δt, and are therefore sufficient to ensure a well-behaved numerical solution.

8. Artificial viscosity

The flow in the z-direction is arbitrary and will depend on the nature of the pressure distribution in z alone. Thus compression flow in z may occur, with shocks in extreme cases. More generally a longitudinal nonlinear oscillatory growth may take place, rather similar in nature to the effects observed in two-dimensional Lagrangian codes. To overcome these problems we introduce an artificial viscosity with stress q into the Lagrangian equation of motion (22):

$$\frac{\partial w}{\partial t} = -\frac{1}{M}\frac{\partial}{\partial z}\{XY(p_0+q_0)\}, \tag{35}$$

where the stress

$$q = \begin{cases} a^2\rho\dfrac{\partial(\Delta z)^2}{\partial t} & \left(\dfrac{\partial w}{\partial z} < 0\right), \\ 0 \quad \text{(otherwise)}, \end{cases} \tag{36}$$

a being a constant, and Δz an effective cell width. The artificial viscosity in this form satisfies the hybrid condition since q/ρ is a function of (z,t) only. q_0 is the value of q on the axis.

In finite-difference form q is

$$q_{i+\frac{1}{2}}^{n+\frac{1}{2}} = \left\{ \begin{array}{ll} \tfrac{1}{2}a^2(\rho_{i+\frac{1}{2}}^n+\rho_{i+\frac{1}{2}}^{n+1})\,(W_{i+1}^{n+\frac{1}{2}}-W_i^{n+\frac{1}{2}})^2 & (W_{i+1}^{n+\frac{1}{2}} < W_i^{n+\frac{1}{2}}), \\ 0 \quad \text{(otherwise)}, & \end{array} \right\} \tag{37}$$

and the equation of motion

$$W_i^{n+\frac{1}{2}} = W_i^{n-\frac{1}{2}} - \frac{2\Delta t[X_{i+\frac{1}{2}}^n\, Y_{i+\frac{1}{2}}^n(p_{i+\frac{1}{2}}^n+q_{i+\frac{1}{2}}^n) - X_{i-\frac{1}{2}}^n\, Y_{i-\frac{1}{2}}^n(p_{i-\frac{1}{2}}^n+q_{i-\frac{1}{2}}^n)]}{M_{i-\frac{1}{2}}+M_{i+\frac{1}{2}}} \tag{27a}$$

The equation of energy balance must be modified to take into account the work done by the artificial viscosity. Thus (23) becomes

$$\frac{\partial E_t}{\partial t} + p_0\frac{\partial \tau_0}{\partial t} + \frac{q_0}{\rho_0}\frac{1}{\Delta z}\frac{\partial(\Delta z)}{\partial t} = w - \frac{\partial Q}{\partial z}. \tag{23a}$$

In a similar fashion the finite-difference equation (32) must also include this term:

$$\begin{aligned} E_{i+\frac{1}{2}}^{n+1} = E_{i+\frac{1}{2}}^n &- \tfrac{1}{2}(p_{i+\frac{1}{2}}^{n+1}+p_{i+\frac{1}{2}}^n)\,(\tau_{i+\frac{1}{2}}^{n+1}-\tau_{i+\frac{1}{2}}^n) \\ &- q_{i+\frac{1}{2}}^{n+\frac{1}{2}}\frac{(X_{i+\frac{1}{2}}^{n+1}\, Y_{i+\frac{1}{2}}^{n+1}+X_{i+\frac{1}{2}}^n\, Y_{i+\frac{1}{2}}^n)\,(Z_{i+1}^{n+1}-Z_{i+1}^n-Z_i^{n+1}+Z_i^n)}{Z_{i+1}^{n+1}+Z_{i+1}^n-Z_i^{n+1}-Z_i^n}. \end{aligned} \tag{32a}$$

This modification is subject to a further stability condition of the form (Richtmyer & Morton 1967, p. 350)

$$\frac{4a^2|\Delta z_{i+\frac{1}{2}}^{n+1}-\Delta z_{i+\frac{1}{2}}^n|}{\Delta z_{i+\frac{1}{2}}^n} < 1 \tag{38}$$

to give for the complete stability condition

$$\Delta t\left\{c\left[\frac{1}{2X^{n^2}}+\frac{1}{2Y^{n^2}}+\frac{1}{\Delta z^{n^2}}\right]^{\frac{1}{2}} + 4a^2\frac{|w_{i+1}^{n+\frac{1}{2}}-w_i^{n+\frac{1}{2}}|}{\Delta z^n}\right\} \leqslant 1, \tag{34a}$$

which must be satisfied in every cell.

9. Thermal conduction

Thus so far we have neglected thermal conduction along the z-direction, which leads to a redistribution of energy. Since the gas is assumed isothermal in the x- and y-directions, the heat flux in the z-direction across a complete (x, y)-cross-section is

$$\mathscr{L} = -\int K \frac{\partial T}{\partial z} \mathrm{d}x\, \mathrm{d}y, \tag{39}$$

where the integral is performed over the complete cross section. This procedure is unsatisfactory for the important case of a plasma, where the thermal conductivity is independent of density, and therefore (x, y), since the Gaussian distribution extends to infinity in the (x, y)-plane. This unphysical behaviour is due to two incorrect assumptions.

(i) The distribution is finite, the Gaussian distribution being in error near the plasma edge. We define the plasma surface by the edge factor Γ such that the boundary is described by the ellipse

$$\frac{x^2}{X^2} + \frac{y^2}{Y^2} = \frac{1}{\Gamma^2}. \tag{40}$$

(ii) Equation (39) assumes that the heat flow is described by Fourier's law. However, at low density, flux limitation occurs, which reduces the heat flux below that calculated using the classical thermal conductivity. A useful approximation for the flux-limited conductivity is:

$$K = \frac{K_0}{1 + \lambda |\nabla T|/T}, \tag{41}$$

where K_0 is the classical conductivity. The empirical constant λ is inversely proportional to density. Hence, if λ_0 is the value on the axis,

$$\lambda = \lambda_0(z, t) \exp\left\{\frac{x^2}{X^2} + \frac{y^2}{Y^2}\right\}. \tag{42}$$

Using (41) and (42) we obtain

$$\mathscr{L} = -\pi X Y K_0 \frac{\partial T}{\partial z}\left\{\Gamma^{-2} - \ln \frac{1 + \lambda_e |\nabla T|/T}{1 + \lambda_0 |\nabla T|/T}\right\}, \tag{43}$$

where $\lambda_e = \lambda_0 \exp \Gamma^{-2}$ is the value of λ at the plasma boundary.

In this calculation we have specifically treated the case of a plasma; the generalization to other media is straightforward and may be accomplished in a similar way. The averaged thermal flux used in (19) and (23) is simply obtained:

$$Q = \frac{\mathscr{L}}{\pi m (1 - \exp[-\Gamma^{-2}])}. \tag{43a}$$

The heat flux Q may be added to (32) in a finite-difference form. As usual in these problems stability requirements demand that the heat transport be treated by an implicit form if stringent timestep limitation is to be avoided (Richtmyer & Morton 1967, p. 187). The problem then reduces to a tridiagonal matrix equation, whose solution is well known (Richmyer & Morton 1967, p. 199).

10. Expansion of large-aspect-ratio cylinders

Before proceeding to the computational tests of the finite-difference scheme proposed in §9, it is convenient to examine the free expansion of cylinders of hot gas into vacuum. The general aspects of this behaviour can be established by a consideration of the characteristics of the hybrid model noted earlier, before recourse is made to numerical integration. In this section we shall examine this motion with reference to the flow of cylinders of circular cross section, for which analytic expressions can be obtained. However, it should be remembered that these results are quite general in nature, and that the conclusions will apply to cylinders of arbitrary cross section.

We consider the expansion of a cylinder of gas of radius R_0 and length $2L_0$. The gas is initially heated, with an internal energy E_0 per unit mass, and no further energy is communicated to it. The motion may be qualitatively described in terms of rarefaction waves propagating from the surfaces into the gas. If the aspect ratio L_0/R_0 is large the radial expansion will be well developed by the time the axial rarefaction has penetrated a distance $\approx R_0$. Thus qualitatively we may expect that a cylindrical expansion is well developed over the bulk of the gas up to a distance $\approx R_0$ from the end, with an approximately spherical expansion from the end. In fact the axial rarefaction continues to propagate into the radial expansion, producing a more uniformly distributed axial velocity: indeed we shall show that in the final asymptotic phase the gas has all acquired a finite axial velocity (except at the origin).

Let us consider the propagation of the head of the axial rarefaction within the hybrid approximation. Neglecting longitudinal thermal conduction the head of the rarefaction must follow the leading characteristic of the hybrid equations into the gas, i.e. since $w = 0$ at the head

$$\frac{\mathrm{d}z}{\mathrm{d}t} = -c.$$

However, the sound speed c varies in time due to the radial expansion, thus, since the expansion is adiabatic,

$$c = c_0\left(\frac{\rho}{\rho_0}\right)^{\frac{1}{2}(\gamma-1)} = c_0\left(\frac{R_0}{R}\right)^{\gamma-1}, \tag{44}$$

where ρ_0 is the initial density and c_0 the initial sound speed. Before the arrival of the first characteristic the motion is purely radial, for which the similarity model equations have the form

$$\frac{1}{\gamma-1}R\frac{\mathrm{d}^2R}{\mathrm{d}t^2}+\left(\frac{\mathrm{d}R}{\mathrm{d}t}\right)^2 = \frac{E_0}{\Psi} = \frac{2}{\gamma(\gamma-1)}\frac{c_0^2}{\Gamma^2}, \tag{45}$$

where $\Psi = \frac{1}{2}\Gamma^2$ is the parameter defined in Pert (1980). This equation has the first integral

$$\left(\frac{\mathrm{d}R}{\mathrm{d}t}\right)^2 = U_0^2+\frac{E_0}{\Psi[1-(R_0/R)^{2(\gamma-1)}]}, \tag{46}$$

where U_0 is the initial (zero) velocity of the perimeter. The motion is therefore described before the arrival of the first characteristic by

$$c_0 t = \left(\frac{2\gamma}{\gamma-1}\right)^{\frac{1}{2}} R_0 \int_1^{(R/R_0)^{1/f}} \frac{z^{f+1}\,\mathrm{d}z}{(z^4-1)^{\frac{1}{2}}}, \tag{47}$$

where $f = 2/(\gamma-1)$ is the number of degrees of freedom of the gas molecules. The distance travelled by the first characteristic is

$$L_0 - z = \int c\,\mathrm{d}t = c_0 \int \left(\frac{R_0}{R}\right)^{\gamma-1} \mathrm{d}t$$

$$= \left(\frac{2\gamma}{\gamma-1}\right)^{\frac{1}{2}} \Gamma R_0 \int_1^{(R/R_0)^{1/f}} \frac{z^{f-1}\,\mathrm{d}z}{(z^4-1)^{\frac{1}{2}}}. \tag{48}$$

The integrals may be evaluated in terms of elliptic integrals if f is integral. In particular, if $f = 3$, $\gamma = \frac{5}{3}$

$$t = \frac{\sqrt{5}}{3}\Gamma R_0 \left\{\left(\frac{R}{R_0}\right)^{\frac{1}{3}} \left\{\left(\frac{R}{R_0}\right)^{\frac{4}{3}} - 1\right\}^{\frac{1}{2}} + \sqrt{\tfrac{1}{2}} F\left[\cos^{-1}\left(\frac{R_0}{R}\right)^{\frac{1}{3}} \middle| \tfrac{1}{4}\pi\right]\right\} \tag{49}$$

$$\approx \frac{\sqrt{5}}{3}\Gamma R_0 \left\{\frac{R}{R_0} + \tfrac{1}{4}(2\pi)^{\frac{1}{2}}\Gamma(\tfrac{1}{4})^2\right\} = \frac{\sqrt{5}}{3}\Gamma R_0 \left\{\frac{R}{R_0} + 1.3110\right\} \tag{50}$$

at large times ($R \gg R_0$), and

$$L_0 - z = \sqrt{5}\,\Gamma R_0 \left\{\left(\frac{R_0}{R}\right)^{\frac{1}{3}} \left\{\left(\frac{R}{R_0}\right)^{\frac{4}{3}} - 1\right\}^{\frac{1}{2}} - \sqrt{2}E\left[\cos^{-1}\left(\frac{R_0}{R}\right)^{\frac{1}{3}} \middle| \tfrac{1}{4}\pi\right] + \sqrt{\tfrac{1}{2}} F\left[\cos^{-1}\left(\frac{R_0}{R}\right)^{\frac{1}{3}} \middle| \tfrac{1}{4}\pi\right]\right\}$$

$$\approx \sqrt{5}\,\Gamma R_0 \left\{\left(\frac{R}{R_0}\right)^{\frac{1}{3}} - \frac{1}{(2\pi)^{\frac{1}{2}}}\Gamma(\tfrac{3}{4})^2\right\} = \sqrt{5}\,\Gamma R_0 \left\{\left(\frac{R}{R_0}\right)^{\frac{1}{3}} - 0.59991\right\} \tag{51}$$

at large times. $F[\ ]$ and $E[\ ]$ are elliptic integrals of the first and second kinds respectively. At large times ($R \gg R_0$) (47) and (48) take the forms

$$c_0 t \approx \left(\frac{\gamma(\gamma-1)}{2}\right)^{\frac{1}{2}} \Gamma R, \tag{47a}$$

$$L_0 - z \approx \frac{1}{2-\gamma}[\tfrac{1}{2}\gamma(\gamma-1)]^{\frac{1}{2}} \Gamma R_0 \left(\frac{R}{R_0}\right)^{2-\gamma}. \tag{48a}$$

It is clear from (48) that, provided that $f \geqslant 2$ (or $\gamma \leqslant 2$), the characteristic continues to propagate inwards for all times. The entire cylinder eventually acquires a longitudinal velocity (except at the centre $z = 0$), and the density distribution will be modified by the axial expansion. The asymptotic distribution will only be reached for times satisfying the inequality

$$c_0 t \gg (2-\gamma) L \left\{(2-\gamma)\left[\frac{2}{\gamma(\gamma-1)}\right]^{\frac{1}{2}} \frac{L}{\Gamma R_0}\right\}^{(\gamma-1)/(2-\gamma)}. \tag{52}$$

The motion of the head of the rarefaction is given in parametric form by (47) and (48): figure 3 shows this motion for various values of γ.

The pattern of flow indicated by this analysis is generally found in numerical calculations, namely that, at a point a distance l from one end, the flow is cylindrical for a time $\approx l^3/15 c_0 \Gamma^2 R_0^2$ ($\gamma = \frac{5}{3}$), after which axial motion occurs and significantly modifies the longitudinal density profile. The motion of the rarefaction head, and therefore the development of the axial profile clearly depend on Γ, the similarity parameter. Figure 4 shows the trajectory of the head in a gas of $\gamma = \frac{5}{3}$ for two typical values of the parameter Γ, clearly demonstrating this effect, and we must expect that simulations using the hybrid model will be sensitive to this parameter.

It is noteworthy that (47) constitutes a complete analytic solution to the problem of the self-similar flow of an instantaneously heated body in cylindrical geometry.

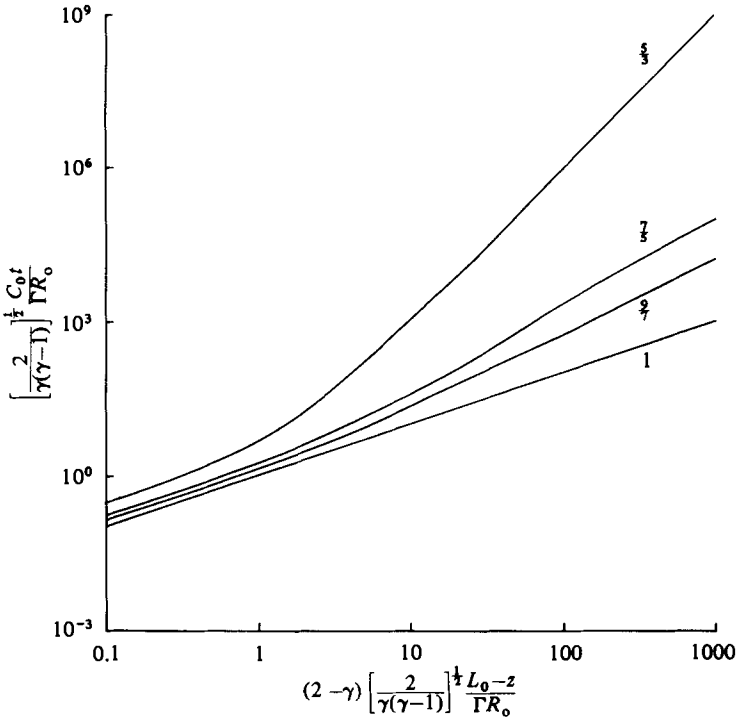

FIGURE 3. The trajectory of the first characteristic propagating along a cylinder for values of $\gamma = 1, \frac{9}{7}, \frac{7}{5}, \frac{5}{3}$.

11. Numerical tests

We may identify three major sources of inaccuracy in calculations using the hybrid model: the local approximation, numerical errors and the representation error. The first of these we have already examined in some detail, and have shown that provided the aspect ratio is not small the error involved is not severe. The second error, that arising from the finite-difference integration techniques described earlier, can be investigated by comparing results from the computer code with known exact analytic solutions of the hybrid equations; for example, the hybrid model reduces to the ellipsoidal similarity flow when the gas-density distribution is Gaussian in the z-direction also. For such flows the true solution may be simply evaluated and indeed some exact integrals of the flow do exist. In particular we may remark on the linear nature of the velocity distribution in z as a good test of the accuracy of the numerical solution. For a polytropic gas of $\gamma = \frac{5}{3}$ with a spherical symmetric density distribution, there exists the following analytic solution for an expansion into vacuum with no energy input and starting from rest:

$$R^2 = R_0^2 + \tfrac{4}{3} E_0 t^2, \tag{53}$$

where R and R_0 are the 1/e radii at times t and 0 as defined earlier (Pert 1980), and E_0 the total (constant) energy.

Figures 5 and 6 show the results of such a test. The hybrid code was used to model the expansion of a spherical Gaussian mass of gas whose $\gamma = \frac{5}{3}$ with boundary radius 1 unit and 1/e radius $R_0 = 0.366$ units. The initial specific energy was 0.667 units. The mesh was constructed with a uniform spacing of 80 cells in the z-direction.

Figure 5 shows the behaviour of the 1/e widths in the x- (or y-) and z-directions,

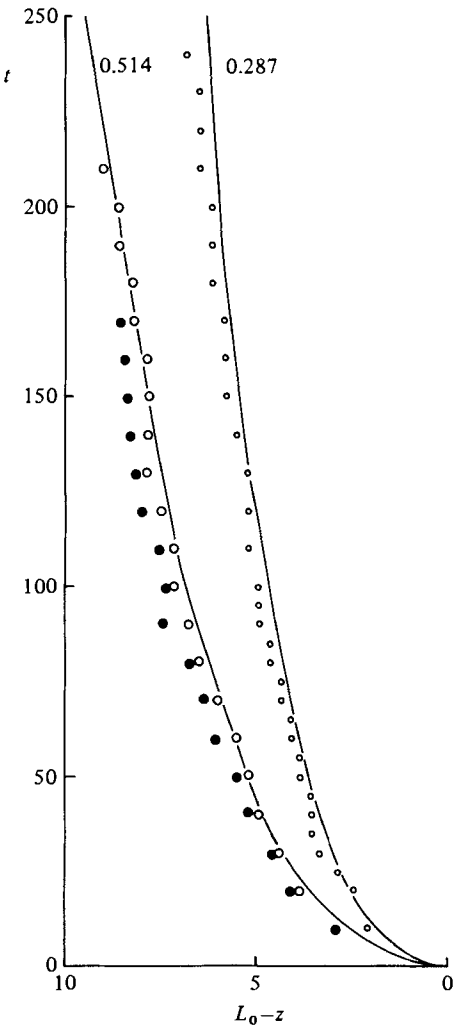

FIGURE 4. The trajectories of the first characteristic calculated analytically (——) for values of $\Gamma = 0.287$ and 0.514, are compared with the finite-difference calculation (○). Also shown are values measured from the 2-dimensional code (●) calculations. The cylinder had an initial radius 1 unit, specific internal energy 1 unit, and the gas $\gamma = \frac{5}{3}$.

X and Z respectively, calculated with the code as functions of t^2. It can be seen that to a high degree of accuracy

$$X = Z = R, \tag{54}$$

where R is given by (53). The slightly larger value of Z is reflected in the correspondingly smaller value of X. The origin of the error in Z is due to the truncation error of the numerical scheme. In figure 6 we plot the expansion velocity w in the z-direction in terms of the Lagrangian parameters i characterizing the cell boundary. Since the mesh had initially uniform spacing, the similarity model predicts that w should be a linear function of i. Figure 6 shows that this condition is accurately maintained up to cell 70, but that thereafter there is a progressive, but small, error up to the edge. Such a departure is only to be expected and of course, results from the violation of the similarity condition at the edge of the mesh, where a vacuum is assumed. The development of this edge zone can be observed in the difference

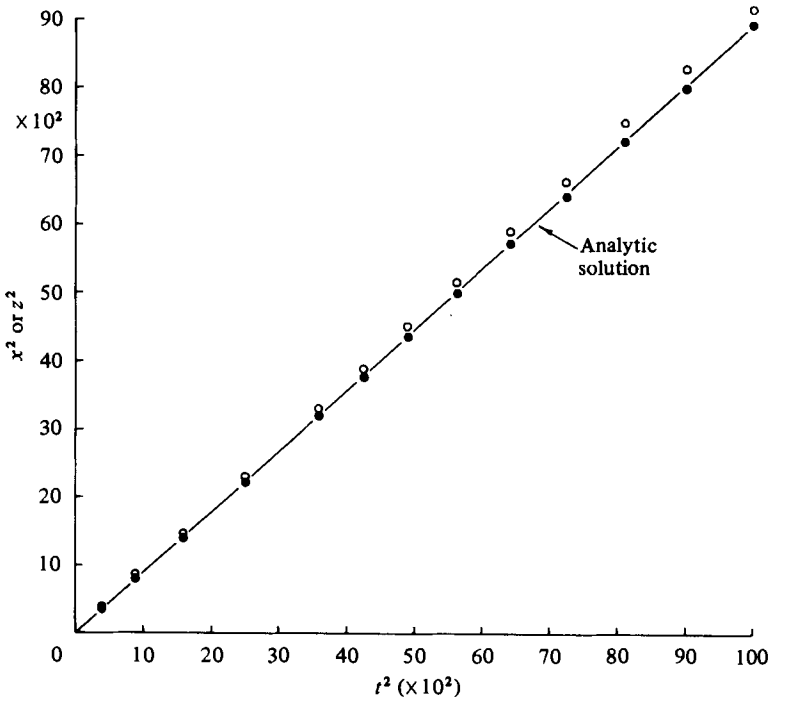

FIGURE 5. The development of the axial z (○) and radial x (●) 1/e widths of a Gaussian distribution sphere with time t. The analytic solution is represented by the linear relationship between the squares of the 1/e widths and time.

between the asymptotic velocity profile (at $t = 100$) and the profiles at times 0.1, 0.5 and 1.0.

A further test of the numerical accuracy of the finite-difference form is shown in figure 4, where we compare the motion of the head of the rarefaction propagating down the cylinder, calculated from (47) and (48) with values obtained from the code. Bearing in mind the inaccuracies in the latter in identifying the head, the agreement is remarkably good.

In practice we shall be interested in calculating the flow of uniform, but limited, gas masses. The representational error is due to the use of an approximate functional density profile to represent a more complex real one, and is likely in all cases of practical importance to be the dominant inaccuracy. Regarding this term we may immediately place some bounds on its range for rod-shaped bodies, for it is clear that, as the rod length becomes very large, the expansion is purely symmetric, and the solution that of the cylindrical similarity model, whose accuracy is given in our earlier paper (Pert 1980). Furthermore, at the limit of small aspect ratios $\epsilon \approx 1$ we may consider the sphere, which was also treated earlier. This latter problem may be considered as a worst case, for, being a short 'stumpy' body, the errors in the axial expansion may be expected to reduce as the aspect ratio is increased, and the expansion becomes more cylindrical. A good idea of the reliability of the model for representing these flows can therefore be obtained by consideration of our earlier detailed treatment of the similarity model, and of a spherical expansion. We shall therefore examine this latter case in some detail.

We compare the flow of a sphere of radius 1 unit, density 1 unit and energy density 1 unit, calculated with a one-dimensional spherical symmetric Lagrangian code using

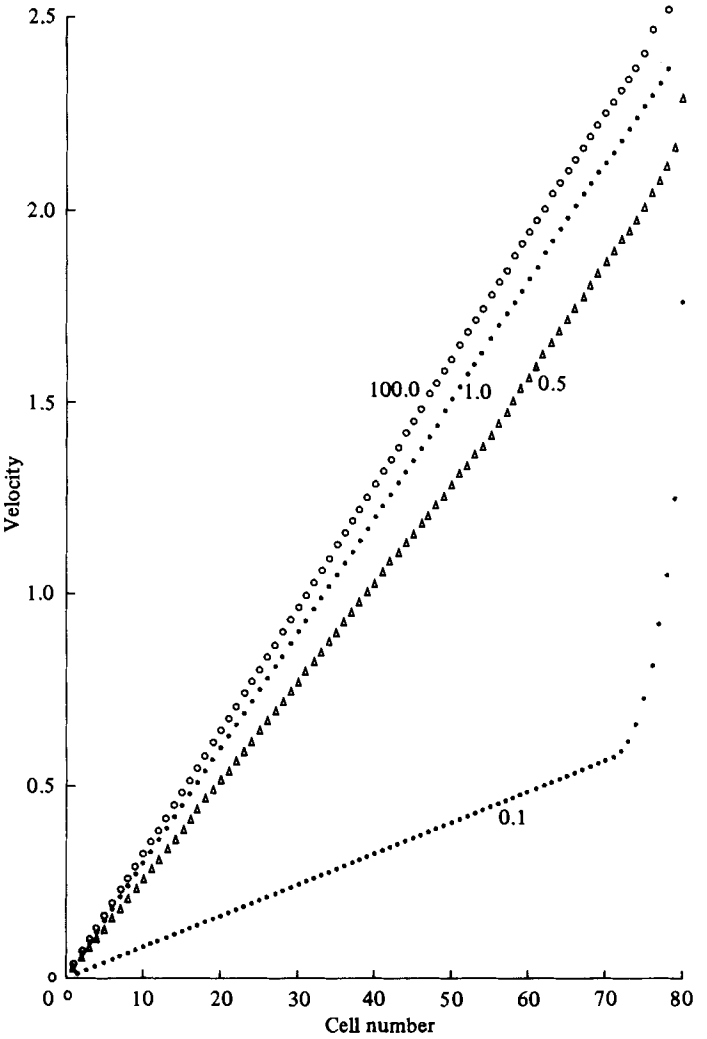

FIGURE 6. The variation of the axial velocity with Lagrangian cell parameter i at various times during the expansion of a sphere with Gaussian density distribution.

91 cells, with that calculated by the hybrid code using 80 cells. We may remark that this flow being spherically symmetric is not hybrid, and further that this provides a more severe problem than those expected to be encountered in practice where the aspect ratio of the axial to radial dimensions is large. Examination of the results presented in Pert (1980) shows that the greatest deviation from a similarity expansion occurs in the case of a gas with $\gamma = \frac{5}{3}$, which case we therefore use as a test. As in our earlier work (Pert 1980) it is necessary to match the boundary of the sphere to the initial 1/e width of the equivalent similarity profile, through a parameter Γ defined as in (48). In this case we match the initial values of X and Y for each cell to the appropriate boundary value of the sphere in that cell using a constant value of Γ. Appropriate values of Γ for matching the expansion of an isothermal sphere to an equivalent similarity flow were deduced in Pert (1980), two differing values being obtained for different matching conditions.

Figures 7 and 8 show comparison of the flows calculated with the hybrid model and with the Lagrangian code. In each case we compare the results obtained with the two values (0.247 and 0.456) of the matching parameter derived in Pert (1980).

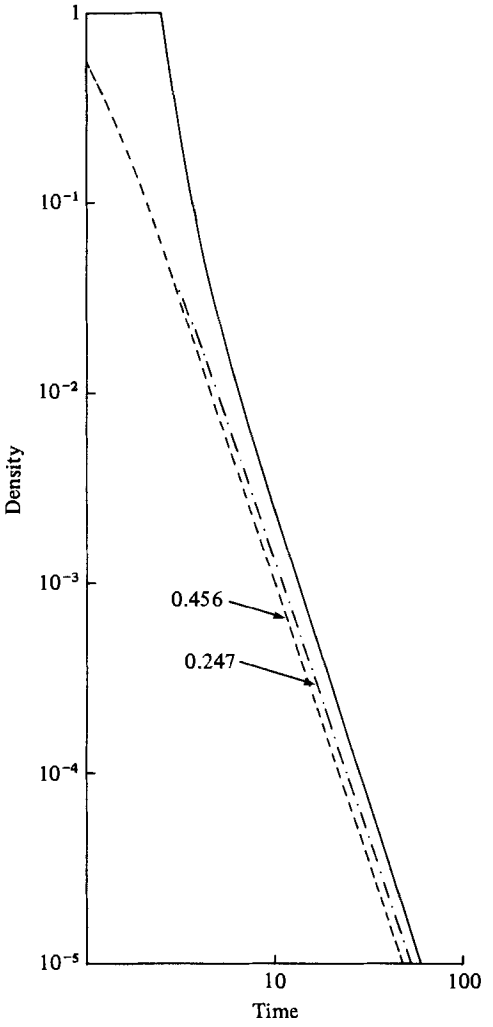

FIGURE 7. Variation of the density at the centre of an initially uniform sphere of gas expanding into vacuum, calculated with a 1-dimensional Lagrangian code (——) and with the hybrid code using two different values of the similarity parameter Γ.

In figure 7 we show the behaviour of the central density as a function of time. It can be seen that except during the initial phase of expansion as a rarefaction propagates in towards the axis the central density is well described. In the hybrid code it is necessary to include a limit of the form given earlier (Pert 1979) to describe the early rarefaction wave phase, namely

$$\rho_{i+\frac{1}{2}} = \left\{ \begin{array}{ll} \dfrac{M_{i+\frac{1}{2}}}{x^0_{i+\frac{1}{2}} y^0_{i+\frac{1}{2}} (z_{i+1} - z_i)} & (X < x^0_{i+\frac{1}{2}};\ Y < y^0_{i+\frac{1}{2}}), \\ \dfrac{2}{\pi^{\frac{1}{2}}} \dfrac{M_{i+\frac{1}{2}}}{x^0_{i+\frac{1}{2}} Y_{i+\frac{1}{2}} (z_{i+1} - z_i)} & (X < x^0_{i+\frac{1}{2}};\ Y \geqslant y^0_{i+\frac{1}{2}}), \\ \dfrac{2}{\pi^{\frac{1}{2}}} \dfrac{M_{i+\frac{1}{2}}}{X_{i+\frac{1}{2}} y^0_{i+\frac{1}{2}} (z_{i+1} - z_1)} & (X \geqslant x^0_{i+\frac{1}{2}};\ Y < y^0_{i+\frac{1}{2}}), \\ \dfrac{M_{i+\frac{1}{2}}}{X_{i+\frac{1}{2}} Y_{i+\frac{1}{2}} (z_{i+1} - z_1)} & (X \geqslant x^0_{i+\frac{1}{2}};\ Y \geqslant y^0_{i+\frac{1}{2}}), \end{array} \right\} \tag{55}$$

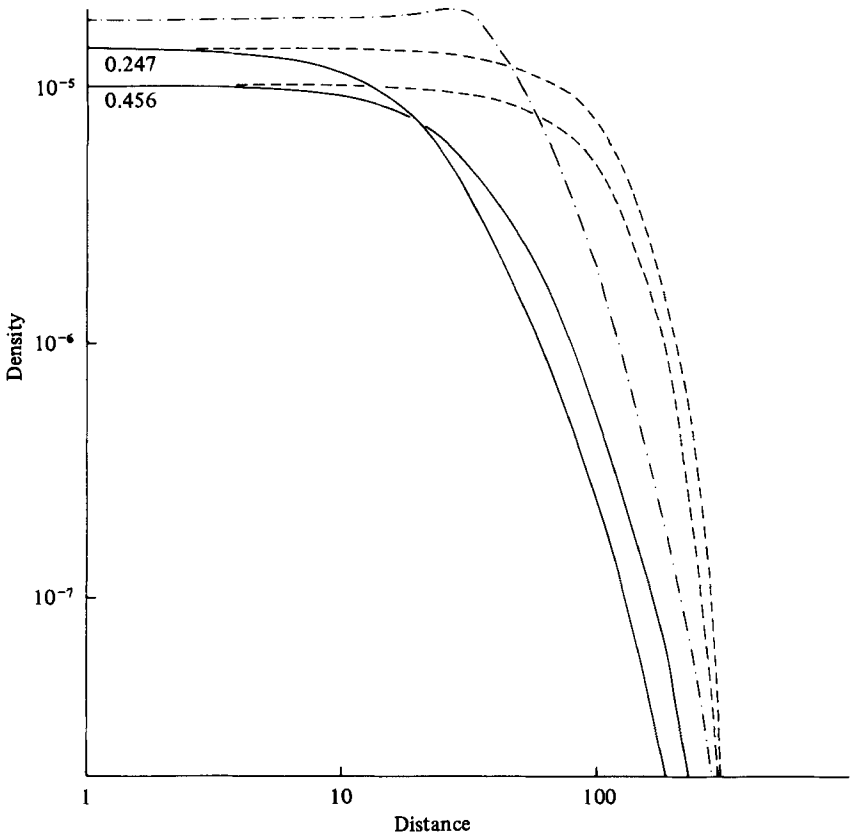

FIGURE 8. Comparison of the density profiles of an initially uniform sphere expanding into vacuum calculated at late times (asymptotic form) in the axial (——) and radial (– – – –) directions by the hybrid code with two different values of the similarity parameter Γ. For reference the profile given by a 1-dimensional Lagrangian fluid code calculation is also shown (—·—·—).

when $x^0_{i+\frac{1}{2}}$ and $y^0_{i+\frac{1}{2}}$ are the initial boundary dimensions in the x-and y-directions respectively. As can be seen (figure 7) it is this phase of the motion which is poorly described.

In figure 8 we compare the late-time density profile calculated with the hybrid model with that evaluated by the Lagrangian code. It can be seen that the actual profile is reasonably accurately represented by the model, although the unusual behaviour near the centre remarked in our earlier work is not reproduced. The overall representation is, however, markedly more accurate than that of the simple similarity flow. From figure 8 we may note that the accuracy of the representation near the origin is improved as Γ is decreased, whereas the converse is true over most of the profile. Furthermore, the symmetry of expansion is better maintained with $\Gamma = 0.456$. In general, $\Gamma = 0.456$ appears to be a good compromise for this problem and to give the best representation overall.

The spherical expansion, although a useful test case in that an accurate solution is available, is rather artificial in that its aspect ratio is small. More realistic tests must involve the calculation of flows of large-aspect-ratio cylinders, a more severe problem involving at least a two-dimensional code. For these tests the recently developed quasi-Lagrangian method (Pert 1983) was finally adopted. Initial tests with a fully Lagrangian two-dimensional code showed that, although the code worked

well, the implicit assumption in the hybrid model of uniform transverse temperature could not be maintained and led to marked deviations between the calculations. The use of an orthogonal mesh with rezoning overcame this difficulty, but introduced another by virtue of the rezoning. In particular, initial calculations using the SHASTA algorithm were characterized by a severe fourth-order diffusion of the radial velocity near the axis and led to a badly distorted radial density profile. This was avoided by the use of the donor cell (with flux correction) algorithm, which, for a quasi-Lagrangian system, minimizes the fourth-order diffusion, but gave rise to some errors, as will be noted.

One of the major objectives of this series of the two-dimensional code runs was to determine a suitable value of the similarity constant to match the hybrid model. As we have seen, the motion of the rarefaction head is sensitive to variations in this parameter. Figure 4 includes the trajectory of this characteristic measured during the expansion of a preheated cylinder of gas ($\gamma = \frac{5}{3}$) of unit radius, unit density and unit specific energy; the length was 10 units. The head of the rarefaction could be clearly identified for about the first 150 units of time, before diffusion obscured its location. It can be clearly seen that the motion is compatible with $\Gamma = 0.514$, but not with $\Gamma = 0.287$, and indicates a value of Γ perhaps slightly greater than the former. This result, and the preceding, indicate that the parameter Γ_d, and not Γ_e, as defined earlier (Pert 1980) should be used. This is believed to be a general result, as the former quantity characterizes the bulk flow within which the rarefaction travels, whereas the latter depends on the edge.

A number of comparison runs have been performed. The results from them are all very comparable, and we therefore examine only one specific case, namely a circular cylinder of gas, $\gamma = \frac{5}{3}$, radius 1 unit, length 5 units, initial density 1 unit and energy density 1 unit, at a specific time in the flow, 200 units after initiation, when the flow is well developed. The hybrid calculations were performed with similarity parameters of 0.287 and 0.514 and used 48 cells: the 2-dimensional code used a mesh of 48×23 cells. A quadratic zone distribution (Pert 1983) was used in both codes to improve the accuracy.

A study of the axial velocity distribution in both codes at this time showed that the motion was nearly asymptotic ($w \sim z/t$) everywhere. Furthermore the variation of axial velocity across the radial plane was everywhere less than 3 % in conformity with the local approximation, and was greatest at the tail of the expansion, where the errors are largest.

A comparison of the longitudinal density profiles (figure 9) shows that for $\Gamma = 0.514$ there is no significant error on-axis and that the averaged density distribution is calculated to a reasonable degree of accuracy. The distribution at a radius of 221.0 corresponds approximately to the $\frac{1}{2}$ point of the similarity distribution and to cell 13 of the code. We may also note the error in the tail of the expansion calculated on axis with the 2-dimensional code of the type noted elsewhere (Pert 1983).

The origin of the small error off axis is seen by examining the radial distribution profiles (figure 10*a*). Comparison with the equivalent charts for cylindrical expansion (Pert 1980) shows that the error arises from the representation error of the underlying cylindrical expansion by a similarity profile, and is no more severe than is found there. It is perhaps interesting to note that, near the axis, the density has a Gaussian profile, but with a 1/e width significantly less than that given by the similarity model (figure 10*b*).

Comparing the results of the two-dimensional code calculation with the hybrid results for the two values of the parameters 0.287 and 0.514, it can be seen (figures

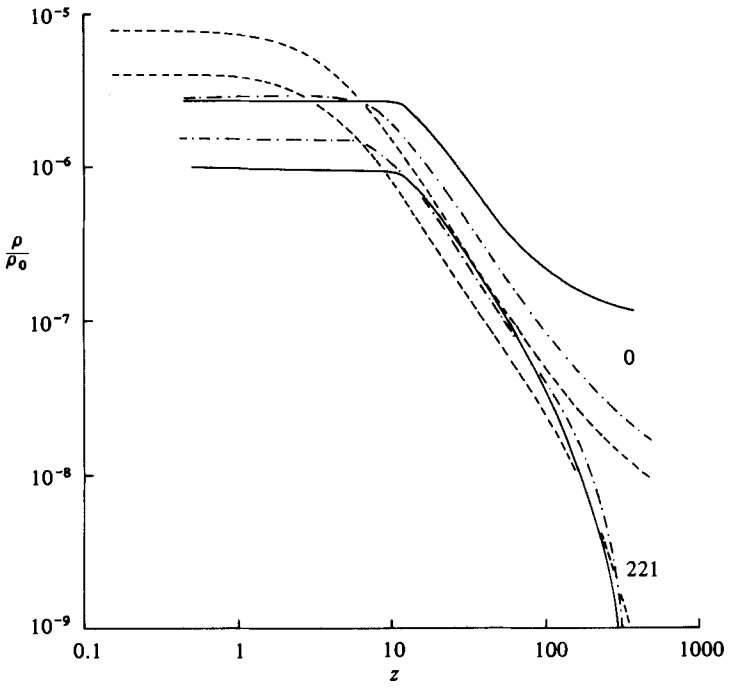

FIGURE 9. Comparison of the axial density profiles calculated with 2-dimensional code (——) and the hybrid model for $\Gamma = 0.287$ (– – – –) and $\Gamma = 0.514$ (— · — · —), on axis and at radius of 221 units, at time 200 units during the expansion of a cylinder radius 1 unit and length 5 units, initial specific energy 1 unit.

9 and 10) that the larger value of Γ gives markedly more accurate results, in agreement with our earlier analysis based on the motion of the leading characteristic, and confirms that Γ_d and not Γ_e should be used.

It may be expected that the accuracy of the model will improve if the gas is slowly heated over a time comparable to the radial expansion time R_0/c_0, in analogy with the corresponding result for pure similarity flows (Pert 1980). Numerical checks using the two-dimensional codes confirm that this is indeed the case, and that the results are broadly in line with our earlier predictions.

As a final example we examine a problem in which shock compression occurs to illustrate the effect of the artificial viscosity. The problem chosen is more extreme than those of more practical interest, in that the cylinder has an aspect ratio length/diameter of only unity, and is instantaneously heated over a small local region. We consider a symmetric problem about the (x, y) axial plane through the centre of the cylinder, and study only the right half-plane. The cylinder initially has a half-length of 1 unit and radius 1 unit, the density and specific energy are 1 and 10^{-8} units respectively. The half-cylinder is represented by a hybrid model with 80 cells along its length, and with a matching parameter $\Gamma = 0.456$. At a time $t = 0$, the centre cell (i.e. $z = \pm 0.0125$) is instantaneously heated to a specific energy of 1 unit: the other cells remaining cold. We consider only the hydrodynamic aspects of the problem, neglecting any thermal conduction along the axis. The artificial viscosity constant a^2 was set to 2.

The flow in this case may be expected to resemble a blast wave moving along the cylinder, with a simultaneous radial expansion. The model predicts just such a behaviour, and figure 11 shows the variation of density along the cylinder axis after

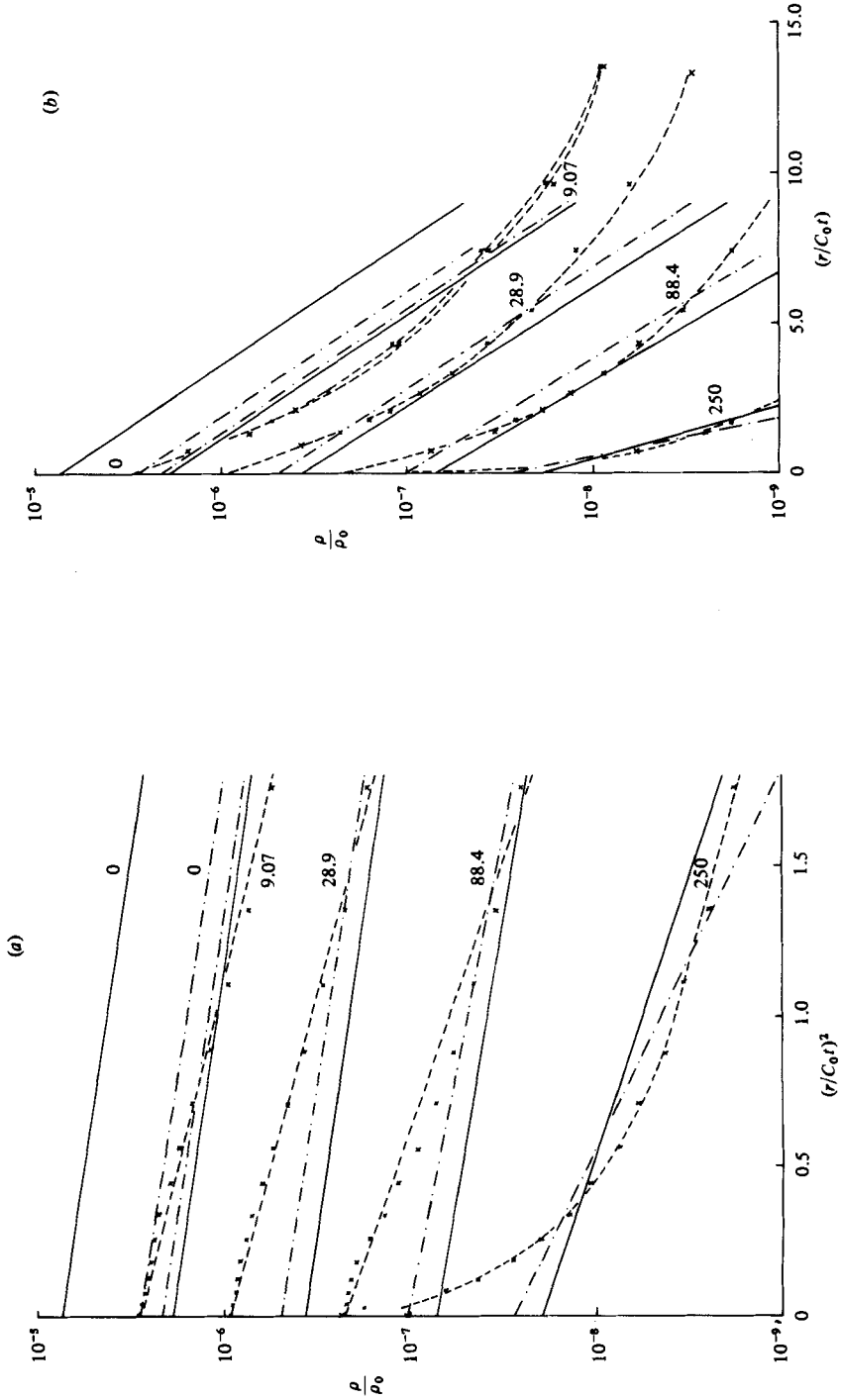

FIGURE 10. Comparison of the radial density profiles during the expansion of figure 9, calculated by the 2-dimensional code (×, – – –) and the hybrid code with $\Gamma = 0.287$ (——) and $\Gamma = 0.514$ (— · — · —).

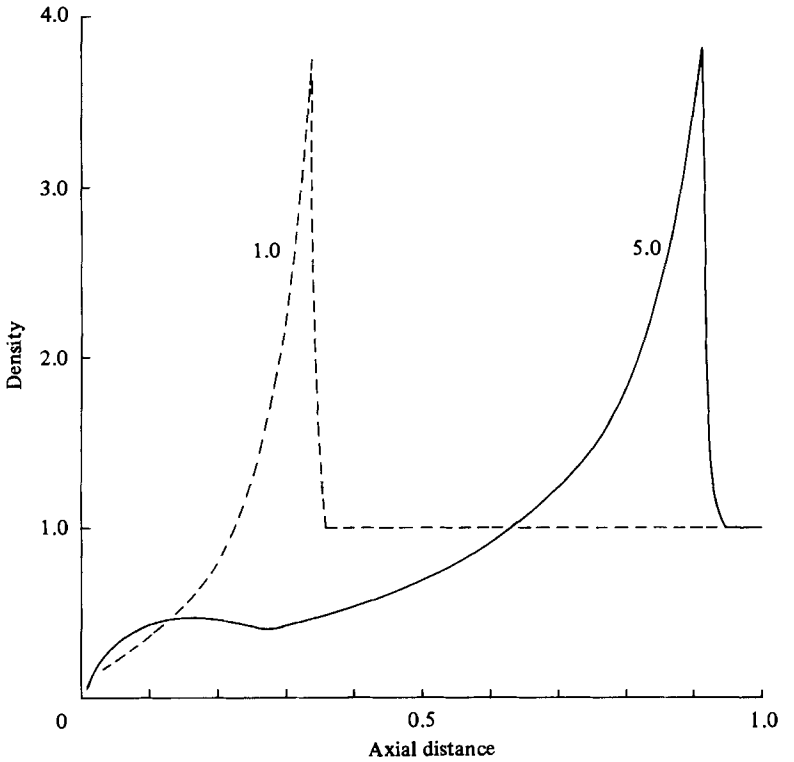

FIGURE 11. The axial flow of a cylinder of length and diameter 2 units locally heated in the centre only. The profiles are shown at times 1 unit (----) and 5 units (——).

times of 1 unit and 5 units. As can be seen, a strong shock followed by a rarefaction propagates along the cylinder. The compression ratio ≈ 3.8 across the shock may be compared with the exact value for a planar strong shock of 4.0. The subsequent expansion of shock-heated gas rapidly leads to the large density decrease behind the shock. In the later stages of expansion some backstreaming occurs along the axis near the centre to fill the void left by the more rapid expansion of hotter gas in this region.

The smooth profile of the shock in figure 11 should be noted, indicating the satisfactory nature of the artificial viscosity term used. The shock front thickness of about 3 cells is compatible with the value of a^2 used in this test (Richtmyer & Morton 1967, p. 317).

12. Conclusion

A model for examining the expansion of non-uniformly heated thin gas cylinders has been examined. It is based on an exact solution of the equations of hydrodynamics involving the separation of variables into a two-dimensional similarity system and a one-dimensional flow. The method can be considerably extended in its applicability by the introduction of a local approximation which is valid for a wide range of cylindrical flows, typically aspect ratios greater than 2. A simple test allows the validity of the local approximation to be routinely assessed. The numerical integration of the model has been described, and its accuracy assessed by comparison with solutions independently obtained.

The application of the hybrid model to real flows is accomplished by means of the matching parameters Γ, which express the ratio of the initial dimension of the real flow to the equivalent scale length (1/e width) of the similarity expansion. In purely symmetric systems the error introduced by a poor value of the matching parameter is relatively small. In contrast we have shown that, in a hybrid flow, this parameter determines the motion of the rarefaction head, and therefore must be reasonably accurately known. It is found by several numerical tests that a good match is obtained if the value used is the bulk parameter Γ_d of Pert (1980).

The hybrid model used in this work has involved an isothermal linear self-similar flow, for which an exact solution exists. The application of the model is considerably extended by the use of the local approximation, which is remarkably accurate. This hybrid model also allows shock propagation along the axis. Other hybrid models no doubt exist; for example, a one-dimensional isothermal linear similarity flow and cylindrically symmetric motion describes the expansion of thin circular disks of very small aspect ratio. The use of alternative similarity forms is probably somewhat limited, for most do not yield an exact solution. Only the local approximation exists, and is markedly less accurate, not being based on an exact form. In addition other forms do not contain a shock solution. The linear isothermal form thus appears in many respects unique. Nonetheless it does provide a simple, inexpensive approach for those problems to which it can be applied, and which can otherwise only be tackled by large and complex computer codes. In view of the latter problems, less accurate alternative hybrid models may find application using local approximations with a check on the accumulated error.

It is difficult to assess the overall accuracy of the representation of a specific problem by the hybrid model in the absence of detailed exact or experimental results. The comparison with the essentially two-dimensional modelling described here shows that it is capable of reasonable accuracy for large-aspect-ratio expansions. As can be seen from the data presented the accuracy decreases markedly as the aspect ratio approaches unity. Although the tolerable error obviously varies from problem to problem, further numerical tests show that a reasonable degree of accuracy can be expected for aspect ratios greater than about 3 (for which the local approximation is well upheld). At smaller values the results should be interpreted with some degree of caution.

The hybrid model has been used to investigate the expansion of thin carbon fibres following irradiation by non-uniform laser beams, where the power deposited varies relatively slowly over distances of the order of the fibre diameter. In these calculations it is assumed that the radial isothermal condition is upheld by thermal conduction, but axial temperature variations are allowed. In this connection we may remark that, since the heat is deposited relatively slowly, Nemchinov's hypothesis (Pert 1980) ensures that the transverse density will closely approximate to a Gaussian over most of the fibre.

This work was performed as part of the XUV laser programme and is supported by SERC.

Appendix A. Energy conservation on the mesh

We consider the total energy at half-integer timesteps defined by

$$\epsilon^{n+\frac{1}{2}} = \sum_i \tfrac{1}{2} M_{i+\frac{1}{2}} (E^n_{ti+\frac{1}{2}} + E^{n+1}_{ti+\frac{1}{2}}) + \tfrac{1}{4} M_{i+\frac{1}{2}} ((U^{n+\frac{1}{2}}_{i+\frac{1}{2}})^2 + (V^{n+\frac{1}{2}}_{i+\frac{1}{2}})^2) + \tfrac{1}{4} (M_{i-\frac{1}{2}} + M_{i+\frac{1}{2}}) (W^{n+\frac{1}{2}}_i)^2$$

with boundary values defined appropriately. We wish to obtain the difference in the total mesh energy over one timestep:

$$\begin{aligned}\epsilon^{n+\frac{1}{2}}-\epsilon^{n-\frac{1}{2}} = \sum_i & -\tfrac{1}{4}M_{i+\frac{1}{2}}[(p^{n+1}_{i+\frac{1}{2}}+p^{n}_{i+\frac{1}{2}})(\tau^{n+1}_{i+\frac{1}{2}}-\tau^{n}_{i+\frac{1}{2}})+(p^{n}_{i+\frac{1}{2}}+p^{n-1}_{i+\frac{1}{2}})(\tau^{n}_{i+\frac{1}{2}}-\tau^{n-1}_{i+\frac{1}{2}})]\\ & +\tfrac{1}{4}M_{i+\frac{1}{2}}[U^{n+\frac{1}{2}}_{i+\frac{1}{2}}+U^{n-\frac{1}{2}}_{i+\frac{1}{2}})(U^{n+\frac{1}{2}}_{i+\frac{1}{2}}-U^{n-\frac{1}{2}}_{i+\frac{1}{2}})+(V^{n+\frac{1}{2}}_{i+\frac{1}{2}}+V^{n-\frac{1}{2}}_{i+\frac{1}{2}})(V^{n+\frac{1}{2}}_{i+\frac{1}{2}}-V^{n-\frac{1}{2}}_{i+\frac{1}{2}})]\\ & +\tfrac{1}{4}(M_{i-\frac{1}{2}}+M_{i+\frac{1}{2}})(W^{n+\frac{1}{2}}_{i}+W^{n-\frac{1}{2}}_{i})(W^{n+\frac{1}{2}}_{i}-W^{n-\frac{1}{2}}_{i}).\end{aligned}$$

Making use of the finite-difference relations we obtain, after some algebra,

$$\begin{aligned}\epsilon^{n+\frac{1}{2}}-\epsilon^{n-\frac{1}{2}} = \sum_i & -\tfrac{1}{4}M_{i+\frac{1}{2}}[(p^{n+1}_{i+\frac{1}{2}}-p^{n}_{i+\frac{1}{2}})(\tau^{n+1}_{i+\frac{1}{2}}-\tau^{n}_{i+\frac{1}{2}})-(p^{n}_{i+\frac{1}{2}}-p^{n-1}_{i+\frac{1}{2}})(\tau^{n}_{i+\frac{1}{2}}-\tau^{n-1}_{i+\frac{1}{2}})]\\ & -\tfrac{1}{2}p^{n}_{i+\frac{1}{2}}[\{X^{n+1}_{i+\frac{1}{2}}\,Y^{n+1}_{i+\frac{1}{2}}\Delta z^{n+1}_{i+\frac{1}{2}}-(X^{n}_{i+\frac{1}{2}}\,Y^{n}_{i+\frac{1}{2}}\Delta z^{n}_{i+\frac{1}{2}}+X^{n}_{i+\frac{1}{2}}\,Y^{n}_{i+\frac{1}{2}}(W^{n+\frac{1}{2}}_{i+1}-W^{n+\frac{1}{2}}_{i})\Delta t\\ & +X^{n}_{i+\frac{1}{2}}\,V^{n+\frac{1}{2}}_{i+\frac{1}{2}}\Delta t\,\Delta z^{n}_{i+\frac{1}{2}}+U^{n+\frac{1}{2}}_{i+\frac{1}{2}}\Delta t\,Y^{n}_{i+\frac{1}{2}}\Delta z^{n}_{i+\frac{1}{2}})\}\\ & -\{X^{n-1}_{i+\frac{1}{2}}\,Y^{n-1}_{i+\frac{1}{2}}\Delta z^{n-1}_{i+\frac{1}{2}}-(X^{n}_{i+\frac{1}{2}}\,Y^{n}_{i+\frac{1}{2}}\Delta z^{n}_{i+\frac{1}{2}}\\ & -X^{n}_{i+\frac{1}{2}}\,Y^{n}_{i+\frac{1}{2}}(W^{n-\frac{1}{2}}_{i+1}-w^{n-\frac{1}{2}}_{i})\Delta t-X^{n}_{i+\frac{1}{2}}\,V^{n-\frac{1}{2}}_{i+\frac{1}{2}}\Delta t\,\Delta z^{n}_{i+\frac{1}{2}}-U^{n-\frac{1}{2}}_{i+\frac{1}{2}}\Delta t\,Y^{n}_{i+\frac{1}{2}}\Delta z^{n}_{i+\frac{1}{2}})\}],\end{aligned}$$

neglecting contributions from the boundary. Comparing terms it can be seen that the residual terms are of order Δt^3, and that the scheme is therefore weakly conservative (see Pert 1981, §III). In this case it can be shown that subject to a timestep constraint limiting the fractional conservation error increase per timestep, the total error over the complete integration is bounded by a term of order Δt. Since the kinetic energy is necessarily non-negative, and the internal energy positive if (33) is satisfied, both terms must themselves be bounded. Hence the system is formally stable (Richmyer & Morton 1967, pp. 45 and 132).

This condition is, however, not entirely satisfactory for the value of the fractional conservation error remains arbitrary. The problem may be identified by requiring that no growth of an error in the solution occurs. This can only be analysed in terms of test solutions (cf. Gear 1971, p. 9). Such a solution is that of an initially uniform state with a sinusoidal error, i.e. the normal-mode analysis given in appendix B, whose results are complementary to those of the energy analysis (cf. Richtmyer & Morton 1967, p. 133). The condition that the fractional error term be not greater than the original perturbation leads to a condition essentially the same as (B 15).

Appendix B. Linear stability of the finite-difference scheme

We consider the response of the finite-difference equations to a single Fourier component of the error in the representative form

$$\delta p = \tilde{p}\exp\{\mathrm{i}\delta j\} \tag{B 1}$$

for a term p with Lagrangian index j. Linearizing the finite-difference equations with respect to this perturbation we obtain the amplification matrix $\boldsymbol{G}$ for the error in the terms $(\tilde{x}^1, \tilde{y}^1, \tilde{z}^1, \tilde{u}^{\frac{1}{2}}, \tilde{v}^{\frac{1}{2}}, \tilde{w}^{\frac{1}{2}})$ in the forms

$$(\tilde{x}^1, \tilde{y}^1, \tilde{z}^1, \tilde{u}^{\frac{1}{2}}, \tilde{v}^{\frac{1}{2}}, \tilde{w}^{\frac{1}{2}}) = \boldsymbol{G}(\tilde{x}^0, \tilde{y}^0, \tilde{z}^0, \tilde{u}^{-\frac{1}{2}}, \tilde{v}^{-\frac{1}{2}}, \tilde{w}^{-\frac{1}{2}}), \tag{B 2}$$

where $\boldsymbol{G}$ is given in table 1 in terms of the sound speed $c = (\gamma p^0/\rho^0)^{\frac{1}{2}}$. As is well known, the equations (B 2) are linearly stable if the eigenvalues λ of $\boldsymbol{G}$ have magnitude less than unity (Richtmyer & Morton 1967, p. 68), i.e.

$$|\lambda| \leqslant 1. \tag{B 3}$$

$1-\frac{2c^2\Delta t^2}{(x^0)^2}$	$-\left(\frac{\gamma-1}{\gamma}\right)\frac{2c^2\Delta t^2}{x^0y^0}$	$-2i\left(\frac{\gamma-1}{\gamma}\right)\frac{2c^2\Delta t^2}{x^0\Delta z^0}\sin\delta$	Δt	0	0
$-\left(\frac{\gamma-1}{\gamma}\right)\frac{2c^2\Delta t^2}{x^0y^0}$	$\frac{1-2c^2\Delta t^2}{(y^0)^2}$	$-2i\left(\frac{\gamma-1}{\gamma}\right)\frac{2c^2\Delta t^2}{y^0\Delta z^0}\sin\delta$	0	Δt	0
$\frac{2ic^2\Delta t^2}{x^0\Delta z^0}\sin\delta$	$\frac{2ic^2\Delta t^2}{y^0\Delta z^0}\sin\delta$	$\frac{1-4c^2\Delta t^2}{\Delta z^2}\sin^2\delta$	0	0	Δt
$\frac{-2c^2\Delta t}{(x^0)^2}$	$-\left(\frac{\gamma-1}{\gamma}\right)\frac{2c^2\Delta t}{x^0y^0}$	$-2i\left(\frac{\gamma-1}{\gamma}\right)\frac{2c^2\Delta t}{x^0\Delta z^0}\sin\delta$	1	0	0
$-\left(\frac{\gamma-1}{\gamma}\right)\frac{2c^2\Delta t}{x^0y^0}$	$\frac{-2c^2\Delta t}{(y^0)^2}$	$-2i\left(\frac{\gamma-1}{\gamma}\right)\frac{2c^2\Delta t}{y^0\Delta z^0}\sin\delta$	0	1	0
$\frac{2ic^2\Delta t}{x^0\Delta z^0}\sin\delta$	$\frac{2ic^2\Delta t}{y^0\Delta z^0}\sin\delta$	$\frac{-4c^2\Delta t}{(\Delta z^0)^2}\sin^2\delta$	0	0	1

TABLE 1

We may directly evaluate the determinant for the eigenvalues of $\boldsymbol{G}$ to obtain

$$(1-\lambda)^6-P\lambda(1-\lambda)^4+Q\lambda^2(1-\lambda)^2-R\lambda^3=0, \tag{B 4}$$

where

$$P=-(c\Delta t)^2\left\{\frac{2}{(x^0)^2}+\frac{2}{(y^0)^2}+\frac{4}{(\Delta z^0)^2}\sin^2\delta\right\},$$

$$Q=8(c\Delta t)^4\left\{\frac{1}{2}\frac{2\gamma-1}{\gamma^2}\frac{1}{(x^0)^2}(y^0)^2+\frac{1}{\gamma}(\Delta z^0)^2\left[\frac{1}{(x^0)^2}+\frac{1}{(y^0)^2}\right]\sin^2\delta\right\},$$

$$R=-16(c\Delta t)^6\frac{\sin^2\delta}{\gamma^2}\frac{1}{(x^0)^2}(y^0)^2(\Delta z^0)^2. \tag{B 5}$$

We may factorize equation (B 4) to

$$[(1-\lambda)^2+\alpha_1\lambda][(1-\lambda)^2+\alpha_2\lambda][(1-\lambda)^2+\alpha_3\lambda]=0, \tag{B 6}$$

where the values α_1, α_2 and α_3 are roots of the equation

$$\alpha^3+P\alpha^2+Q\alpha+R=0. \tag{B 7}$$

The eigenvalue λ is thus a solution of the quadratic equation

$$(1-\lambda)^2+\alpha\lambda=0, \tag{B 8}$$

whose roots λ_1 and λ_2 must satisfy

$$\lambda_1\lambda_2=1, \quad \lambda_1+\lambda_2=2-\alpha. \tag{B 9}$$

Hence, since $\lambda_1=\lambda_2^*/|\lambda_2|^2$, it is clear that $|\lambda|\leqslant 1$ if α is real and $0\leqslant\alpha\leqslant 4$.

Equation (B 7) with

$$P=-(X+Y+Z), \quad Q=\frac{(X+Y)Z}{\gamma}+\frac{2\gamma-1}{\gamma^2}XY, \quad R=-\frac{1}{\gamma^2}XYZ \tag{B 10}$$

may be reduced to the form

$$(\alpha-X)(\alpha-Y)(\alpha-Z)-f^2(\alpha-X)-g^2(\alpha-Y)-h^2(\alpha-Z)+2fgh=0, \tag{B 11}$$

where

$$f=\left[\frac{(\gamma-1)}{\gamma}YZ\right]^{\frac{1}{2}},\quad g=-\left[\frac{(\gamma-1)}{\gamma}ZX\right]^{\frac{1}{2}},\quad h=\frac{\gamma-1}{\gamma}(XY)^{\frac{1}{2}},\tag{B 12}$$

whose roots are all real (Hall & Knight 1948, p. 487). Comparing (B 10) with (B 5), we see that X, Y, Z are all positive and therefore that f, g and h are real if $\gamma \geqslant 1$. The roots of (B 7) are therefore real if $\gamma \geqslant 1$, and, furthermore, applying Descartes' rule of signs it follows that they are all non-negative.

The cubic (B 7) can only be solved in a simple algebraic form for special cases, for example if $\gamma = 1$

$$\alpha_1=\frac{2}{(x^0)^2}(c\Delta t)^2,\quad \alpha_2=\frac{2}{(y^0)^2}(c\Delta t)^2,\quad \alpha_3=\frac{4\sin^2\delta}{(\Delta z^0)^2}(c\Delta t)^2.$$

Nonetheless we may derive a simple sufficient condition for stability, for, since

$$P=-(\alpha_1+\alpha_2+\alpha_3),$$

the stability condition on the roots, namely $0 \leqslant \alpha \leqslant 4$, is obeyed if

$$(c\Delta t)^2\left\{\frac{1}{2(x^0)^2}+\frac{1}{2(y^0)^2}+\frac{1}{(\Delta z^0)^2}\right\}\leqslant 1,$$

which is an obvious generalization of the usual Courant–Friedrichs–Lewy condition for one-dimensional Lagrangian schemes (Richtmyer & Morton 1967, p. 297).

REFERENCES

Courant, R. & Friedrichs, K. O. 1948 *Supersonic Flow and Shock Waves*. Wiley-Interscience.

Gear, C. W. 1971 *Numerical Initial Value Problems in Ordinary Differential Equations*. Prentice-Hall.

Hall, H. S. & Knight, S. R. 1948 *Higher Algebra*. MacMillan.

Pert, G. J. 1974 *Plasma Phys.* **16**, 1051.

Pert, G. J. 1979 *J. Phys.* B: *Atom. & Mol.* **12**, 2067.

Pert, G. J. 1980 *J. Fluid Mech.* **100**, 257.

Pert, G. J. 1981 *J. Comp. Phys.* **43**, 111.

Pert, G. J. 1983 *J. Comp. Phys.* **49**, 1.

Richtmyer, R. D. & Morton, K. W. 1967 *Difference Methods for Initial Value Problems*. Wiley-Interscience.